ELSEVIER

Fusion Engineering and Design 25 (1994) 215–225

Fusion Engineering and Design

Magnetohydrodynamic stability regimes for steady state and pulsed reactors

S.C. Jardin, C.E. Kessel, N. Pomphrey

Princeton University, Plasma Physics Laboratory, P.O. Box 451, Princeton, NJ 08543, USA

Abstract

A tokamak reactor will operate at the maximum value of $\beta \equiv 2\mu_0\langle p\rangle/B^2$ that is compatible with magnetohydrodynamic (MHD) stability. This value depends on the plasma current and pressure profiles, the plasma shape and aspect ratio, and the location of nearby conducting structures. In addition, a steady state reactor will minimize its external current drive requirements and thus achieve its maximum economic benefit with a bootstrap fraction near unity, $I_{BS}/I_P \approx 1$, which constrains the product of the inverse aspect ratio and the plasma poloidal β to be near unity, $\epsilon\beta_P \approx 1$. An inductively driven pulsed reactor has different constraints set by the steady-state Ohm's law which relates the plasma temperature and density profiles to the parallel current density. We present the results obtained during ARIES I, II/IV, and III and PULSAR reactor studies where these quantities were optimized subject to different design philosophies. The ARIES-II/IV and ARIES-III designs are both in the second stability regime, but differ in requirements in the form of the profiles at the plasma edge, and in the location of the conducting wall. The relation between these, as well as new attractive MHD regimes not utilized in the ARIES or PULSAR studies, is also discussed.

1. Introduction

In order for a plasma equilibrium configuration to be physically realizable, it must be stable to ideal magnetohydrodynamic (MHD) modes of oscillation. This constraint severely limits the class of pressure and current distributions suitable for use in a tokamak based fusion reactor.

The stability constraint comes into play differently for pulsed and for steady-state reactors. For inductively driven pulsed reactors there is very little freedom in the form of the plasma current profile. For a given plasma density and temperature profile, the spatial distribution of the plasma current profile in the flat-top phase of the discharge follows immediately from the neoclassical Ohm's law and the condition that the loop voltage is constant throughout the plasma. This is discussed in more detail in Section 5. The allowable pressure in this configuration is then the maximum pressure that is stable for that current profile.

For a steady-state reactor, there is in principle much more freedom between the form of the current and the pressure profiles since they are somewhat independent. Thus, a designer has the freedom to produce a plasma current profile using external current drive that is favorable for stabil-

SSDI 0920-3796(94)00064-E

ity and thereby allows large values of the plasma pressure. However, in practice we find that because of the low efficiencies of a non-inductive current drive, the penalty for supplying a large fraction of current by external current drive is significant. This leads to a preference for configurations in which most of the plasma current is generated by the plasma itself by the "bootstrap effect", discussed in Section 3. While not an absolute constraint, the economics of steady-state reactors is such that only those pressure and current profiles which make maximum use of the bootstrap effect are acceptable for use in a reactor. This is a different but almost equally constraining condition on these profiles.

In the remainder of this paper, we elaborate on these issues and show how the conclusions are reached. In Section 2 we describe the different stability regimes available to tokamaks. In Section 3 we discuss the plasma bootstrap current and what its scaling is. We then discuss how these considerations lead to specific designs for the plasma physics parameters of steady-state and pulsed reactors in Sections 4 and 5. Section 6 summarizes the main results.

2. First and second stability regimes

Different conditions apply to optimize the performance of a tokamak reactor depending on whether or not it is in the first or second regime of stability with respect to ballooning modes (which do not perturb the plasma boundary) and whether it is being limited by ballooning or by kink modes. We discuss some of the considerations here.

2.1. First stability

Most present day tokamak experiments operate normally in what is called the first stability regime. This is the only stable operating regime available to tokamaks that have centrally peaked current profiles of the kind produced by an ohmic heating transformer in the stationary phase of a pulsed discharge. First stability regime tokamaks are characterized by a safety factor profile $q(\psi)$ that is normally near unity on the magnetic axis, and increases monotonically to a value of at least two, and more typically three or more at the plasma boundary.

First stability regime tokamaks are constrained to operate at values of β below the Troyon limit [1,2].

$$\beta \leq C_T \frac{I_P}{aBq_0} \tag{1}$$

where I_P is the total plasma current, a is the minor radius, B is the toroidal magnetic field on the axis, q_0 is the magnetic safety factor on the axis, and the Troyon coefficient C_T is normally taken to be 3.5. How close a given first stability discharge can come to the β limit in Eq. (1), or in fact whether it can somewhat exceed it, depends largely on the form of the current and the pressure profiles. Detailed, profile-specific stability analysis is necessary to determine the applicable Troyon coefficient for a given discharge. While a review of the profile dependence of the first stability β limit is outside the scope of the present survey, we note here that in general one would expect that the more freedom one has in selecting the plasma current and pressure profiles, the closer one can come to achieving or exceeding the equality in Eq. (1).

2.2. Second stability

It has been known for some time that under certain conditions and at high enough pressure, there exists a "second stable" region with respect to ideal MHD modes that do not perturb the plasma boundary [3–9]. This restabilization is attributed to the strong distortion of the equilibrium magnetic flux surfaces at higher pressures. The large shifting of the flux surfaces to the large major radius side of the tokamak greatly increases the poloidal field on the outboard side. This increases the local pitch of the magnetic field lines so that the plasma spends less time traversing the outboard part of the plasma where the combination of pressure gradient and magnetic field line curvature is unfavorable to stability.

The distortion of the equilibrium also decreases the local magnetic shear on the outboard side of the plasma. The ballooning instability arises where the pressure gradient is large, the magnetic

field line curvature is unfavorable, and the magnitude of the local shear is small or vanishes. If the pressure is high enough, the outward shift of the magnetic axis will cause the local magnetic shear on the outboard side to decrease through zero, creating a region of large negative local shear which is stabilizing. This also forces the zero shear region away from the outboard to a region where the destabilizing combination of pressure gradient and magnetic curvature is much weaker, leading to overall stability. The conventional picture is that at low enough pressure tokamak plasmas will be stable (first stability region) to ballooning modes, at intermediate pressure they become unstable, and at high pressures they become stable again (second stability region). However, under certain conditions it is also possible to find intermediate pressure equilibria that are also stable to $n = \infty$ ballooning modes. If a sequence of stable intermediate pressure equilibria exists, the final state is called "accessible".

A detailed $n = \infty$ ballooning mode analysis must be performed on all internal plasma magnetic surfaces to determine whether a given plasma configuration is in the second stability region. Such studies show that in order for all the surfaces in the plasma to be stable and in the second stability regime, the pressure profile must be sufficiently peaked. With these provisos, we note that the second stability regime is characterized by having the product of the inverse aspect ratio and the poloidal beta $\epsilon\beta_P$ greater than or of the order of unity

$$\epsilon\beta_P \geq 1 \tag{2}$$

where

$$\beta_P \equiv \frac{8\pi^2\langle p\rangle a^2}{\mu_0 I_P^2}\frac{1+\kappa^2}{2} \tag{3}$$

and by having the toroidal beta β much greater than the Troyon value including the factor of q_0 in the denominator,

$$\beta \gg 3.5\frac{I_P}{aBq_0} \tag{4}$$

In addition to these inequalities, one of several additional conditions must be met in order for a stable second stability regime to exist in a plasma. These conditions are as follows:

(1) the plasma cross-section must be strongly bean shaped [8],

(2) the value of the safety factor q must be everywhere greater than 2.0 [9], or

(3) the form of the q-profile must be such that $q(\psi)$ decreases in going from the plasma axis to the plasma edge (negative q') over a significant fraction of the plasma cross section [5,10].

We have not been able to utilize condition (1) in a reactor design, but condition (2) forms the basis for both the ARIES II/IV designs and the ARIES-III advanced fuels design. Condition (3) also holds promise as leading to an attractive reactor design. These are discussed further in Section 4 in the context of steady-state reactors.

2.3. The external kink mode

The other ideal MHD instability of concern is the $n = 1$ external kink mode, which does perturb the plasma–vacuum interface. Although at zero or low values of plasma pressure, kink modes are driven unstable by the parallel current density, at higher pressures they also have strong destabilizing pressure-driven contributions. These pressure-driven external kinks are often called ballooning-kink modes. Generally, a full global MHD calculation (e.g. PEST, GATO, ERATO) must be performed to determine stability; however, some basic guidelines can be followed. The dimensionless quantity

$$\frac{q_*}{q_0} = \frac{\pi a^2 B(1+\kappa^2)}{\mu_0 R I_P q_0} \tag{5}$$

is a cylindrical approximation of the ratio of the global safety factor at the plasma edge to that at the center, and is a measure of the broadness or peakedness of the current density profile. Broad current density profiles (q_*/q_0 small) should be destabilizing to the external kink, while peaked profiles (q_*/q_0 large) are stabilizing. The central safety factor q_0 has an analogous effect on the external kink mode. For q_*/q_0 fixed, raising q_0 can stabilize the kink mode while lowering it is destabilizing.

At high enough values of the plasma β, the pressure driven contributions dominate the current-driven contributions to destabilize the kink mode. In the absence of a nearby conducting

structure, the $n = 1$ ballooning-kink mode will only be stable at values of β that lie under the Troyon limit, Eq. (1). It follows from Eq. (4) that this mode is generally unstable in a plasma which is in the second stability regime with respect to the high-n ballooning modes. Therefore, a nearby conducting wall is an essential ingredient of a high β second stability reactor.

The primary function of the conducting structure is to slow the mode down from the Alfven time scale. The critical wall distance, that is the distance that a superconducting wall contouring the plasma boundary would have to be placed to stabilize the mode, is typically found to be 1.2–1.5 times the minor radius, measured from the plasma center. It follows that a resistive wall must be located at a distance less than this in order to slow the growth time of the kink mode down to the order of the L/R time of the wall, and some additional mechanism is required to stabilize the kink mode indefinitely.

There is mounting experimental and theoretical evidence that toroidal plasma rotation may accomplish this [11]. The plasma rotation in effect makes the resistive wall appear superconducting to the plasma. If the plasma is not rotating, as the plasma attempts to distort owing to the instability, it will induce eddy currents in the surrounding wall. These eddy currents will suppress the distortion, but will decay away and become ineffective on a time scale comparable with the L/R time of the wall. However, if the plasma is rotating, as it distorts it will continue to see a different part of the surrounding wall, a "fresh" patch of conductor in which the distortion will induce new eddy currents that suppress the mode. Thus, the required plasma rotation velocity is estimated to be

$$v_\phi \approx \frac{2\pi R}{\tau_w} \tag{6}$$

where R is the plasma major radius, and τ_w is the resistive magnetic diffusion time of the wall.

3. The bootstrap current

The bootstrap current in a tokamak is the part of the toroidal electrical current that is driven directly by the thermal motion of the particles in the tokamak and hence does not require either a transformer-induced loop voltge or external current drive. The bootstrap current makes both steady-state and pulsed reactors more attractive. In steady-state reactors, optimizing the bootstrap current drive can greatly reduce the need for external current drive, and thus the fraction of the reactor power which is recirculated back into powering the current drive systems. In inductively driven pulsed reactors, the bootstrap current will reduce the transformer supplied loop voltage V_L needed to sustain the discharge for a given current, and thus allow either longer discharge times or smaller, less expensive transformers.

Both the magnitude of the bootstrap fraction, I_{BS}/I_P, and the shape of the bootstrap current density profile $J_{BS}(\psi)$, can depend sensitively on the shape of the plasma profiles. Analytic calculations [12] provide valuable information on such trends. Assuming that the temperature, pressure, and current profiles have the parabolic form

$$\sigma = \sigma_0(1 - r^2/a^2)^{\alpha_\sigma} \tag{7}$$

where $\sigma = T$, n, and J, then the total bootstrap fraction can be written in the form

$$I_{BS}/I_P = \epsilon^{1/2}\beta_P C_{BS}(\alpha_n, \alpha_T, \alpha_J, Z, \epsilon) \tag{8}$$

Fig. 1 shows contour plots of the bootstrap coefficient C_{BS} as a function of α_n and α_T for various values of the current profile peakedness parameter α_J. In these figures, the inverse aspect ratio and the plasma effective charge were fixed at the values $\epsilon = 0.22$ and $Z = 2.0$ respectively. We note the overall trends that C_{BS} is largest for flat current profiles (small α_J) and for peaked density profiles (large α_n) and is relatively insensitive to temperature profiles (α_T).

By combining Eqs. (3), (5), and (8), and by making use of the approximate relation

$$q_*/q_0 = \alpha_J + 1 \tag{9}$$

and by using the equality in Eq. (1), we can rewrite Eq. (8) at the first stability beta limit as

$$I_{BS}/I_P = \frac{0.175}{\sqrt{\epsilon}}(\alpha_J + 1)C_{BS} \tag{10}$$

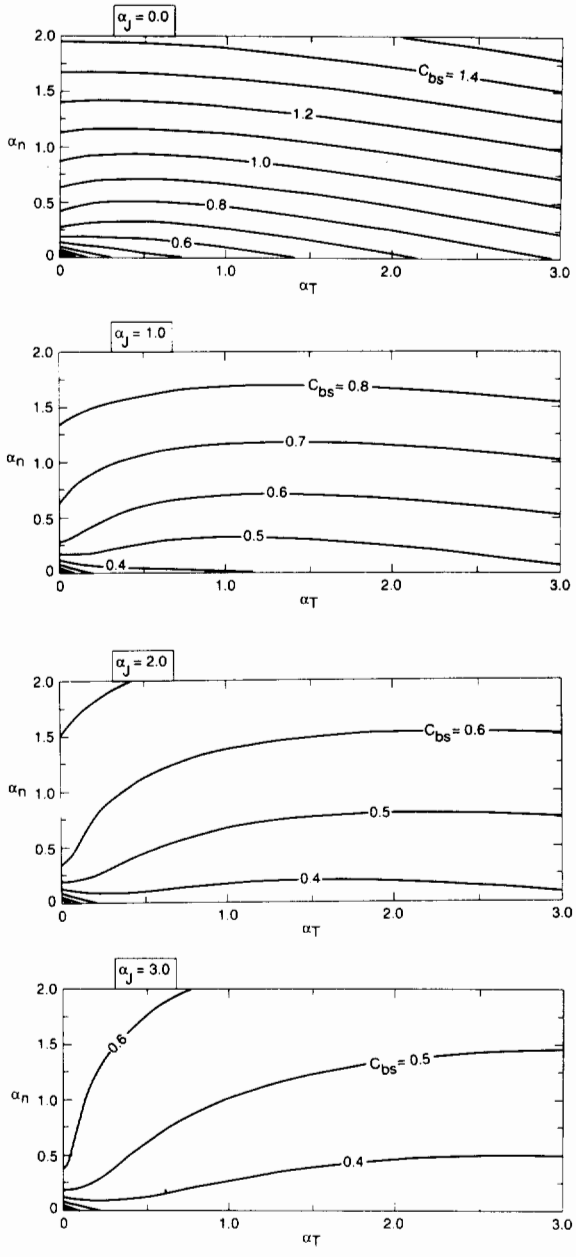

Fig. 1. Contour plots of the bootstrap coefficient C_{BS} in Eq. (8) as a function of α_n and α_T, for selected α_J ($\epsilon = 0.22$, $Z = 2.0$).

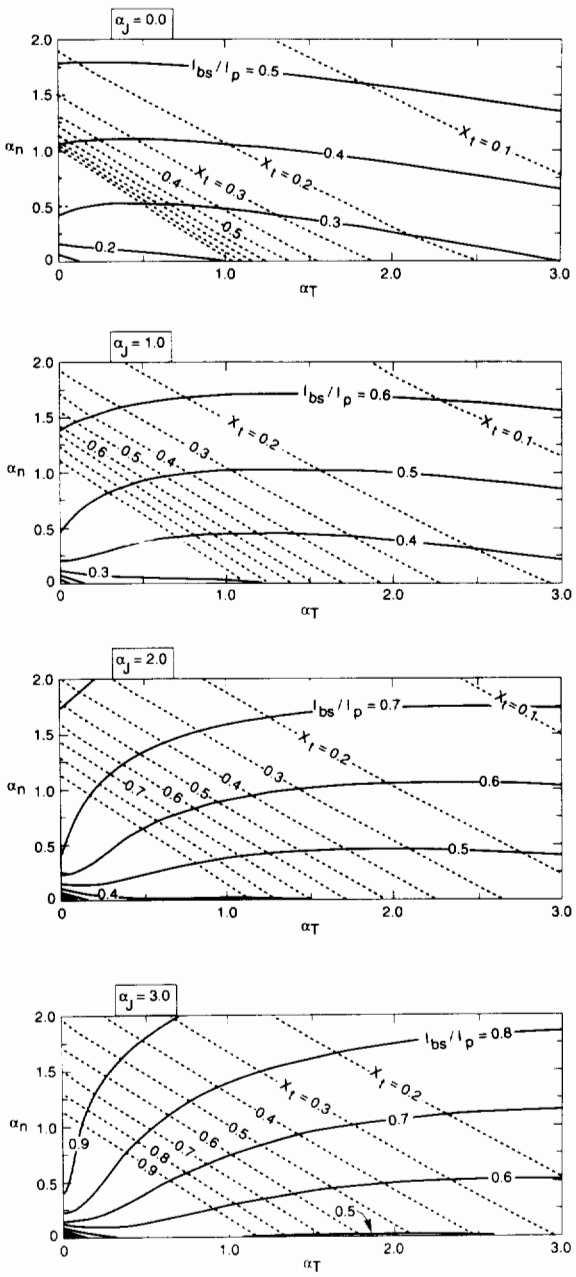

Fig. 2. Contour plots of the bootstrap current fraction I_{BS}/I_P at the first stability regime beta limit as given by Eq. (1). The labeled contour values for I_{BS}/I_P would increase proportional to the factor by which the Troyon limit was exceeded.

Fig. 2 shows (solid) contours of the right hand side of Eq. (10) for the selected values of α_J. Although Eq. (10) and thus Fig. 2 are specialized to plasmas at the first regime beta limit, it is clear that since Eq. (8) was linear in β, it follows that the value of I_{BS}/I_P can be read from Fig. 2 for higher β configurations that exceed the Troyon

limit by some factor by application of a linear scaling.

Choosing to operate in a parameter regime which corresponds to a large bootstrap fraction I_{BS}/I_P is of limited used if the bootstrap-driven profile has the wrong shape. For example, suppose we want to produce a (total) current density profile with a predetermined shape, such as shown in Fig. 3. If the dominant current drive is to be bootstrap, it would clearly be undesirable to generate a bootstrap current density profile $J_{BS}(\psi)$ which peaks near the plasma edge. If this were so, some other means of current drive (such as lower hybrid etc.) would not only have to supply the current deficit at the plasma center to obtain the desired total profile, but also provide reverse drive near the edge. A more desirable shape for the bootstrap current density is shown in Fig. 3(b) where the peak in $J_{BS}(\psi)$ is seen to occur near the plasma center.

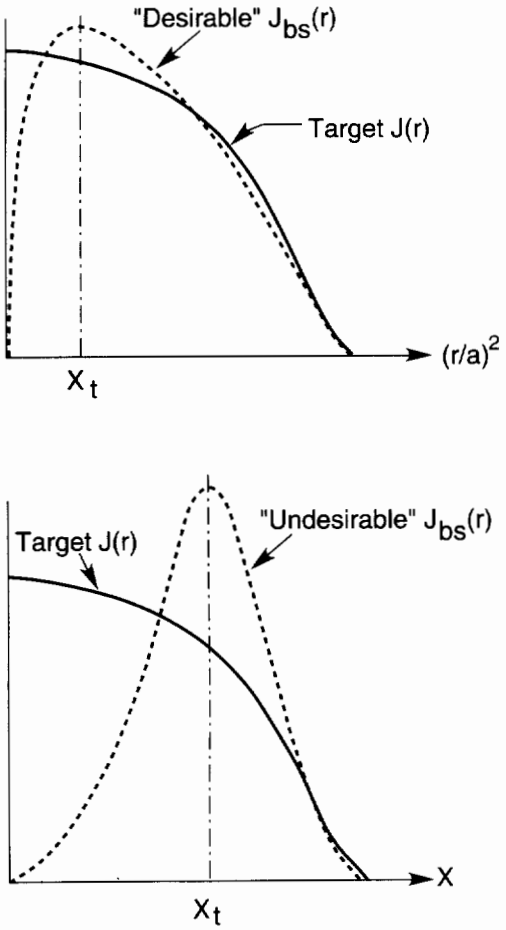

Fig. 3. Schematic picture of "desirable" and "undesirable" bootstrap current profiles J_{BS}. Note that small x_t corresponds to good alignment.

For the parabolic profiles of density, temperature, and current density assumed here, the bootstrap current density is constrained to vanish at the origin ($r = 0$), the plasma edge ($r = a$), and has a single maximum at some intermediate radial location. This implies that once the magnitude of the bootstrap current is specified, the shape of J_{BS} can be characterized by a single parameter, namely the location of the turning point x_t such that $dJ_{BS}(x_t)/dx = 0$. If the total bootstrap fraction is close to unity, we may identify small x_t as being desirable and large x_t as undesirable. The contours of x_t have been superimposed on the plots of I_{BS}/I_P in Fig. 3, thus providing information on a single plot of both shape and magnitude of the bootstrap current.

We can draw several conclusions from Fig. 2. (i) In comparing configurations that are either at the Troyon limit or that exceed it by the same factor, peaked current profiles (large α_J) will have higher bootstrap fractions I_{BS}/I_P than will broad current profiles. (ii) Peaking the density profile (large α_n) increases the bootstrap fraction, but peaking both the density and the temperature profiles (i.e. peaking the pressure profile) aids bootstrap alignment (leads to small x_t as defined in Fig. 3). (iii) In order to achieve bootstrap fractions near 1.0, it is necessary to exceed the first stability regime Troyon limit.

4. Steady-state reactors

It is essential for the economic success of a steady-state reactor that most of the plasma current be supplied by the bootstrap effect. From Eq. (8), we see that this implies that the value of β_P be large. However, for a first stability regime plasma that obeys the Troyon β limit, Eq. (1), large β_P implies low β. This can be seen by recasting the Troyon β limit as

$$(\epsilon\beta_P)(\beta/\epsilon) \leq 0.03\frac{(1+\kappa^2)}{2q_0^2} \quad (11)$$

For a configuration where q_0 and κ are defined, the left-hand side becomes a constant. As β/ϵ is increased, $\epsilon\beta_P$ must decrease and vice versa. This presents the trade-off between increasing β/ϵ to reduce the required toroidal magnetic field, and increasing $\epsilon\beta_P$ to enhance the bootstrap current and reduce the external current drive power. Attempts to increase the right-hand side of Eq. (11) are limited since the plasma elongation κ is constrained to values less than about 2.0 by the $n=0$ vertical instability and the central safety factor q_0 cannot drop too much below unity or internal kink instabilities will set in. A configuration that is in the second stability regime can have simultaneous values of β/ϵ and $\epsilon\beta_P$ that violate the Troyon constraint, Eq. (11). However, as discussed above, this region only exists under certain conditions which themselves limit the operating space for a tokamak plasma.

4.1. ARIES-I

In the ARIES-I reactor study [12], a mode of operation was found which gives a good compromise between high-β and high-β_P while remaining in the first stability regime. Its central safety factor q_0 has been raised to 1.3 while its total current has been reduced from that of a standard tokamak. This configuration has both a high bootstrap fraction for a first stability regime tokamak and a good alignment of the bootstrap current with the plasma current. The ARIES-I design optimized at a value of $\beta = 1.89\%$ and $I_{BS}/I_P = 0.68$ with inverse aspect ratio $\epsilon = 0.22$. The parameters are listed in Table 1.

4.2. ARIES-II/IV and ARIES-III

The ARIES-II/IV configuration is able to exceed the first stability limit to ballooning modes by the fact that it has a sufficiently elevated central safety factor $q_0 > 2$, and sufficiently peaked pressure profile that it is in the second region of stability. The ballooning results are best illustrated in the three-dimensional parameter space $(q_*/q_0, q_0, \epsilon\beta_P)$. Higher values of q_*/q_0 represent peaked current density profiles, and lower values correspond to broad profiles. Shown in Fig. 4 is the q_*/q_0 *vs.* $\epsilon\beta_P$ plane with projections of various q_0 values, showing the stability boundaries to the high-n ballooning modes. For these cases, the current density, pressure, and pressure gradient go to zero at the plasma edge.

Table 1
Parameters used in the ARIES reactor design studies

	ARIES-I	ARIES-II	ARIES-III
q_0	1.3	2.0	2.0
q_*/q_0	3.0	2.30	1.1
β (%)	1.89	3.40	24
I_{BS}/I_P	0.68	0.98	1.16
A	4.5	4.0	3.0
b_{WALL}/a	—	1.25	1.1
I_P (MA)	10.2	6.46	28.5
B_T (T)	11.3	8.01	7.80
R (m)	6.75	5.60	7.50
κ	1.80	2.00	1.85
β_P	2.20	5.40	3.88
β_N	3.20	5.90	16.3

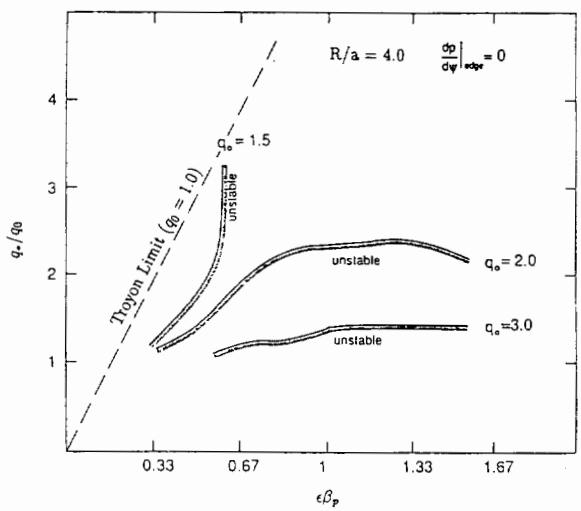

Fig. 4. Stability boundaries in q_*/q_0, $\epsilon\beta_P$ space for $q_0 = 1.5$, 2.0, 3.0. As q_0 is increased from 1.0, it is possible to operate at values of $\epsilon\beta_P$ which exceed the Troyon limit. Contours of constant β/ϵ would increase from the upper left to lower right in this diagram according to Eq. (12).

The diagram indicates that for moderately peaked current profiles (large q_*/q_0) there exist a value of q_0 which allows access to the second stable region. In addition, the diagram shows that as the current profile is broadened (q_*/q_0 is lowered), the value of q_0 needed for access to, or even for the existence of, a second stable region increases.

In terms of the variables used in Fig. 4, the plasma β is given by

$$\beta/\epsilon = \frac{\epsilon\beta_P}{(q_*/q_0)^2}\frac{(1+\kappa^2)}{2q_0^2} \tag{12}$$

This shows that for fixed ϵ, κ, and q_0, β increases from the upper left to the lower right of Fig. 4 but that with other dimensionless parameters held fixed, β decreases with q_0. An additional constraint is that we need $\epsilon\beta_P \approx 1$ for a high bootstrap fraction. These considerations lead to an ARIES II/IV reactor design with $\beta = 3.40\%$, and $I_{BS}/I_P = 0.98$ as shown in Table 1. In comparing ARIES-I with ARIES-II/IV we find that the benefits of second stability are to provide a configuration with about twice the β value and with a bootstrap fraction much closer to unity. Thus, the plasma reactivity would be increased and the amount of recirculating power would be much less for a second stability regime reactor leading to improved economics.

In ARIES-III, β values in excess of 20% are required in order to produce a reactor design for burning the advanced fuels D–^{3}He. We find that such a regime is possible far into the second stability regime but only for a very narrow class of plasma profiles. In particular, we find that the plasma pressure gradients have to remain finite right out to the plasma edge, and that a finite edge plasma current density is also required. This leads to a configuration with $\beta = 24\%$, $I_{BS}/I_P \approx 1.16$, and $q_*/q_0 = 1.1$. Thus the penalty for obtaining these large values of β were that the design was very speculative in that slight variations of the profiles assumed would lead to instability, there was bootstrap overdrive which had to be compensated for with reversed external current drive, and that the conducting walls for stabilizing the external kink modes had to be extremely close. A summary of the parameters of the ARIES reactor designs is given in Table 1.

4.3. Non-monotonic q

This mode seeks to maximize β, and in particular the root mean square average $\beta^* \equiv 2\mu_0\langle p^2\rangle^{1/2}/B^2$ by customizing the pressure and current profiles to allow stable high-β peaked pressure profiles. This is accomplished by distributing the plasma current in such a way that the q-profile provides negative magnetic shear, $dq/d\psi < 0$, in the central region of the discharge. This reversed shear region permits the central part of the discharge to be in the second stable region, allowing the pressure gradients near the center to become very large while remaining stable to ballooning modes. This mode was motivated by high-β negative central shear discharges observed in DIII-D [14], JET [14], and TORE SUPRA [15]. We find that the combination of off-axis current peaking and high β allows for a very good match of the bootstrap and the equilibrium current profiles. An attractive configuration exists with $q_0 = 2.5$, $q_* = 2.35$, $\beta = 4.8\%$, and $\beta^* = 6.33\%$ and with $I_{BS}/I_P \approx 1$. There is an off-axis minimum in q of about 2.1 at $r/a \approx 0.75$. This configuration is a combination of both first and second stability, but still requires a conducting wall at about $1.3a$ to provide for kink mode stability. The theoretical basis for this mode is discussed in Ref. [16] from both an MHD and a kinetic stability viewpoint.

5. Pulsed reactors

In a pulsed reactor, the plasma current is driven by induction from an OH solenoid. There will also be bootstrap current present owing to gradients in the density and the temperature profiles. During flattop, the plasma will be in a steady state so that the current and pressure profiles and other equilibrium quantities are not evolving, and only enough volt-seconds are being supplied by the transformer to compensate for the resistive losses in the plasma.

The parallel plasma current is completely given by the sum of an ohmic part and a bootstrap part. Also, the plasma pressure is a product of density and temperature, $p(\psi) = n(\psi)T(\psi)$. Since for a given magnetic configuration both the ohmic and

bootstrap parts are completely determined by the density and temperature profiles, it follows that steady-state ohmic/bootstrap equilibria like those allowed in an inductively driven pulsed reactor will be completely determined by the density profile $n(\psi)$, the temperature profile $T(\psi)$, and one other quantity which we may take to be either the total plasma current I_P or the central safety factor q_0.

To determine the steady state loop voltage and the maximum stable beta values, we first obtain the corresponding stationary equilibrium solution which is consistent with the parallel Ohm's law, subject to the constant loop voltage constraint. We use the Hirshman single ion formula [17] for bootstrap current in general geometry, extended to include collisional corrections [18]. Thus, the form of the current profile used in the Grad–Shafranov equilibrium calculation is determined from the constraint of being stationary

$$V_L = 2\pi\eta\left[\frac{\langle J\cdot B\rangle}{\langle B\cdot\nabla\phi\rangle} - \frac{\langle J\cdot B\rangle_{BS}}{\langle B\cdot\nabla\phi\rangle}\right] \tag{13}$$

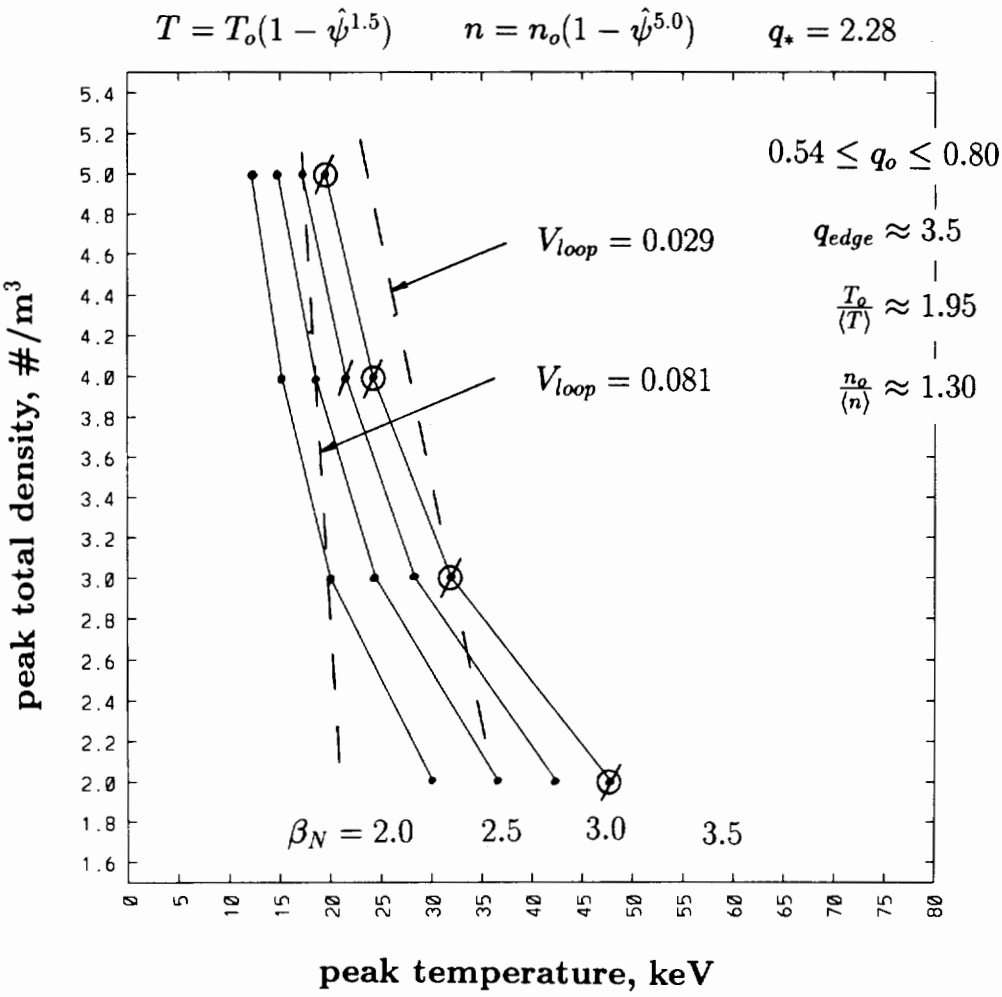

Fig. 5. Stability diagram and loop voltage requirements in POPCON space for an inductively driven pulsed reactor with $I_P = 11.45$ MA, $n(\psi) = n_0(1-\psi^{5.0})^{1.0}$, $T(\psi) = T_0(1-\psi^{1.5})$. Dashed lines show contours of constant loop voltage V_L. Points with dots only are stable to all MHD modes. Open circles indicate instability to external $n = 1$ kink modes, and slashes indicate instability to internal modes.

Here the loop voltage V_L is a constant, η is the neoclassical resistivity [19], ϕ is the symmetry angle in the toroidal direction, and the bootstrap current is defined by

$$\frac{\langle J \cdot B\rangle_{BS}}{\langle B \cdot \nabla\phi\rangle} = -\frac{p_e}{\langle 1/R^2\rangle}\left\{A_1^H\left[\frac{1}{p_e}\frac{dp_e}{d\psi} + \frac{p_i}{p_e}\left(\frac{1}{p_i}\frac{dp_i}{d\psi} - \alpha_i^H\frac{1}{T_i}\frac{dT_i}{d\psi}\right)\right] - \left(\frac{5}{2}A_1^H - A_2^H\right)\left(\frac{1}{T_e}\frac{dT_e}{d\psi}\right)\right\}$$

The superscripts H here refer to coefficients that extend the original values defined in Ref. [17] to those approximating collisional corrections as described in Ref. [19].

We may thus parameterize space easily by varying only the temperature and density profiles and computing the maximum stable β values and the transformer loop voltages V_L for these families of equilibrium. A typical such study is shown in Fig. 5 where we give contours of normalized β_N ($=\beta aB/I_P$), and of V_L for the families of equilibrium with density and temperature profiles given by $n(\psi) = n_0(1-\psi^{5.0})$, $T(\psi) = T_0(1-\psi^{1.5})$.

6. Summary

The MHD stability regime which is appropriate for a given tokamak-based reactor depends on the overall design philosophy of the device. For a steady-state reactor in which there are external current drive sources, there is a strong economic incentive to operate at high β_P to maximize the benefits of the plasma bootstrap current. For a first stability regime tokamak, this implies relatively low β. A second stability regime steady-state reactor may be possible, but is somewhat speculative and would require some nearby conducting structure to stabilize the external kink mode. A high β second stability reactor such as needed to burn advanced fuels is much more speculative, and not as compatible with minimizing the external current drive requirements. A first stability regime inductively driven pulsed reactor does not have to operate at high β_P and so will be able to operate at higher β than a corresponding steady-state reactor. This advantage is partially offset by the loss of flexibility to produce a non-ohmic current profile which would allow operation at a higher normalized beta β_N. Second stability operation is not possible for an inductively driven pulsed reactor because there is no means of modifying the current profile to produce the conditions required.

Acknowledgments

The authors acknowledge valuable contributions from M.S. Chance, D. Ehst, J. Manickam, T.K. Mau, J. Ramos, and L. Zakharov. This work was supported by US DoE Contract No. DE-AC020-76-CHO3073.

References

[1] F. Troyon, R. Gruber, H. Saurenmann et al., Plasma Phys. Controlled Fusion A 261 (1984) 209.
F. Troyon, R. Gruber, H. Saurenmann et al., Phys. Lett. A 110 (1985) 29.
[2] J.J. Ramos, The tokamak $\beta aB/I$ limit and its dependence on the safety factor, Phys. Rev. A 42 (1990) 1021.
[3] B. Coppi, A. Ferreira, J.W. Mark and J.J. Ramos, Ideal-MHD stability of finite-beta plasmas, Nucl. Fusion 19 (1979) 715.
[4] D. Lortz and J. Nuhrenburg, Ballooning-instability boundaries for the circular tokamak, Nucl. Fusion 19 (1979) 1207.
[5] J.M. Greene and M.S. Chance, The second region of stability against ballooning modes, Nucl. Fusion 21 (1981) 453.
[6] J.W. Connor, R.J. Hastie and J.B. Taylor, High mode number stability of axisymmetric toroidal plasmas, Proc. 7th Int. Conf. on Plasma Physics and Controlled Nuclear Fusion Research, Innsbruck, 1979, p. 667.
[7] H.R. Strauss, W. Park, D.A. Monticello, R.B. White, S.C. Jardin, M.S. Chance, A.M.M. Todd and A.H. Glasser, Stability of high-beta tokamaks to ballooning modes, Nucl. Fusion 20 (1980) 638.
[8] M.S. Chance, S.C. Jardin and T.H. Stix, Ballooning mode stability of bean-shaped cross sections for high-β plasmas, Phys. Rev. Lett. 51 (1983) 1963.
[9] M.J. Gerver, J. Kesner and J.J. Ramos, Access to the second stability region in a high shear, low-aspect-ratio tokamak, Phys. Fluids 31 (1988) 2674.
[10] M.S. Chance, S.C. Jardin, C.E.Kessel et al., Ideal MHD stability of very high beta tokamaks, IAEA-CN-53/D-11-1, Proc. 13th Int. Conf. on Plasma Physics and Con-

trolled Fusion Research, Vol. 2, Washington, DC, 1990, IAEA, Vienna, 1991, p. 87.
[11] S. Jardin and T. Taylor (eds.), Workshop on The External Kink Mode and Other MHD Issues, General Atomics Corporation, San Diego, CA, June 1993.
[12] N. Pomphrey, Bootstrap dependence on plasma profile parameters, PPPL-2854, 1992 (Princeton University Plasma Physics Laboratory, Princeton, NJ).
[13] E.A. Lazarus et al., Phys. Fluids B 3 (1991) 2220.
[14] M. Hugo et al., Nucl. Fusion 32 (1992) 33.
[15] Personal communication.
[16] C.E. Kessel, J. Manickam, G. Rewoldt and W. Tang, submitted to Phys. Rev. Lett.
[17] S.P. Hirshman, Phys. Fluids 31 (1988) 3150.
[18] G.R. Harris, Comparisons of different bootstrap current expressions, EUR-CEA-FC-1436, November 1991.
[19] S.C. Jardin, M.G. Bell and N. Pomphrey, Nucl. Fusion 33 (1993) 371.